BOLETIN DE LA SOCIEDAD ESPAÑOLA DE
Cerámica y Vidrio
www.elsevier.es/bsecv

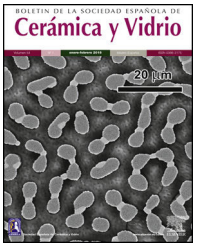

Obtention and characterization of a hybrid nanocomposite monolith by sol–gel process

Maria Celeste Legarto[a,*], *Damian Benito*[a], *Alberto Scian*[a,b], *Maria Barbara Lombardi*[a,b]

[a] *CETMIC, CIC-CONICET, Camino Centenario y 506, M.B.Gonnet 1897, Argentina*
[b] *Depto. de Química, Fac, de Ciencias Exactas, Universidad Nacional de La Plata, Calles 1 y 47, La Plata 1900, Argentina*

ARTICLE INFO

Article history:
Received 22 June 2021
Accepted 21 October 2021
Available online 12 November 2021

Keywords:
Sol–gel
Nanocomposite
Bentonite
Filter bed composite
Water treatment

ABSTRACT

A monolithic porous composite was synthesized by sol–gel process, containing the maximum and significant amount of bentonite that allows its use as a filter bed in aqueous effluents treatment. This process is able to apply on an industrial scale.

The bentonite used was an efficient adsorbent for various contaminant molecules in aqueous media when is operated in a batch stirred tank, but presents difficulty in the separation stage of suspended particles. In this laboratory-scale work, cylindrical monoliths of 9 cm length by 2 cm diameter were made that can be used as a filter bed. The primary composite, silica-resin, was prepared by the sol–gel precursor mixture of the partially hydrolyzed tetraethylorthosilicate and a phenol-formaldehyde resin. Bentonite was added to the pregelling, obtaining the silica-resin-bentonite composite, made up the gel which is then dried and cured at 270 °C. The different composites mineralogical and structurally were evaluated. The preliminary performance of the developed bentonite filter bed showed almost 90% adsorption of diphenylamine, a commercial agrochemical widely used as anti-antiscaldant in postharvest treatment of fruit, and showed that the bentonite conserves its adsorption capacity and controls the swelling of the interlayer space which encourages further research studies applied to water treatment.

Obtención y caracterización de un nanocompuesto monolítico híbrido vía proceso sol-gel

Palabras clave:
Sol-gel
Nanocompuesto
Bentonita
Lecho filtrante compuesto
Tratamiento de aguas

RESUMEN

Se sintetizó vía sol-gel un compuesto híbrido monolítico poroso, con la máxima cantidad significativa de bentonita que permite su uso como lecho filtrante, lo que podría aplicarse en el tratamiento de efluentes acuosos a escala industrial.

La bentonita utilizada es un eficiente adsorbente de varias moléculas de contaminantes presentes en medios acuosos cuando se opera por lotes en tanque agitado, pero presenta la dificultad de separar las partículas suspendidas. Para este trabajo a escala de

* *Corresponding author.*
E-mail address: celestelegarto@cetmic.unlp.edu.ar (M.C. Legarto).
https://doi.org/10.1016/j.bsecv.2021.10.001

laboratorio se realizaron monolitos cilíndricos de 9 cm de largo por 2 cm de diámetro que pueden ser usados como lecho filtrante. El compuesto primario, sílice-resina, se preparó mediante la mezcla precursora sol-gel de tetraetilortosilicato parcialmente hidrolizado y resina fenol-formaldehído. Se añadió bentonita a la mezcla precursora durante la gelificación, para obtener el compuesto sílice-resina-bentonita. Luego del proceso de envejecimiento del gel se cura a 270 °C. Los diferentes compuestos fueron evaluados mineralógica y estructuralmente. El rendimiento preliminar mostró casi el 90% de adsorción de difenilamina, un agroquímico comercial altamente utilizado como antiescaldante en las industrias poscosecha de frutas, y mostró que la bentonita conserva su capacidad de adsorción y controla el hinchamiento del espacio interlaminar, lo que motiva a futuras investigaciones aplicadas al tratamiento de aguas.

Introduction

The most used clay mineral in the synthesis of nanocomposites is montmorillonite, which is the major constituent of bentonite, due to its particula, and unique structure [1–4]. The montmorillonite platelet thickness is only one nanometer, although its dimensions in length and width can be measured in hundreds of nanometers. As it is known, it is a 2:1 aluminosilicate with a crystal structure of one octahedral aluminum centered layer between two tetrahedral silicon-centered [5].

The three layers are interconnected via tetrahedral oxygen tips and octahedral hydroxyl groups and the chemical representation of montmorillonite is $(Na,Ca)_{0.3}(Al,Mg)_2Si_4O_{10}(OH)_2{\cdot}nH_2O$. The isomorphic substitutions occur in both sheets by low valent metal ions, being mainly within the octahedral layer (Mg^{2+}, Fe^{2+}) for Al^{3+} and within the silicate layer (Al^{3+}) for Si^{4+}. This phenomenon gives permanent negative charge on their surfaces which can be balanced by cationic counter-ions occupying interlayer space. These counter-ions, Na^+, H^+, Ca^{2+}, Mg^{2+}, can be exchanged by other cations, thus making them efficient adsorbents for cationic contaminants that may be inorganic like heavy metals or organic like pesticides among many others [6–12].

Due to these ability and efficiency to attract substances, is why they are widely used as adsorbents of toxic compounds and extensively studied in the treatment of effluents [13–22]. The potential product forms of bentonites for effluent treatment involve raw materials, purified, pre-chemical treatment, acid-activated, synthesized, pillared, organically modified, and other complexes containing bentonite [23–28], but the solubilization of these particles in aqueous media is still complex.

Owing to the technical and economical difficulty in the solid/liquid separation, usually there is secondary water pollution, being an undesired feature for their practical use as adsorbents [29–32]. These disadvantages maybe partly explain why most of bentonite and their modified derivatives applications in wastewater treatment remain on a laboratory scale [33]. But adsorption technology is widely considered to be the most promising and robust method to purify aqueous solutions at low cost and with high efficiency [34,35].

An industrial application of adsorption usually involves fixed bed adsorption columns (filter beds) where the adsorbent is continuously in contact with a given quantity of fresh adsorbate. Few studies have reported the use of natural clay as filter beds, although it is a useful technology is not applicable due to practical and operational difficulties [36]. Thus, the interest in a novel hybrid composites that could contain bentonite with the challenge of avoiding the swelling and at the same time retaining the adsorption capacity.

With the purpose of assembling a monolith with or without bentonite, a porous siliceous compound generated by the gelling of TEOS (T) in the presence of different surfactants under various experimental conditions was published in different papers [37–40]. In this paper a hybrid composite was prepared from co-gelling commercial partially hydrolyzed TEOS with phenol-formaldehyde resin (R), which was dried and cured, getting a silica-resin composite (C). The same procedure was followed to prepare the hybrid composite silica-resin-bentonite (C-Bent) but in this case adding the bentonite (Bent) to the sol–gel precursor mixture of T-R. These composites were characterized to elucidate their mineralogical, structural and textural properties.

A preliminary evaluation of the adsorption performance of monolithic composites operating as filter beds for an emerging pollutant [41] was carried out. The emerging pollutant – diphenylamine – was chosen because is widely used in Argentine agroindustry and found in wash water effluents in concentrations that exceed the allowed discharge levels [42].

Materials and methods

Materials

TEOS (T) is an organometallic compound ($Si(CH_3CH_2O)_4$) that when mixed with water and a solvent such as alcohol, is hydrolyzed leading to the formation of a polymeric gel with joints of the type —Si—O—Si—. The chains that are formed by the polymerization generate a three-dimensional crosslinking micelles that lead to the formation of a solid framework that imprisons the water molecules and the rest of the compounds present. The TEOS used (Dynasylan 40 – Evonik Industries) is a partially hydrolyzed mixture of monomers, dimers, trimers, higher polymers and cyclic polysilicates. The average chain length is approximately five units —Si—O—Si—.

Table 1 – Formulation of C and C-Bet.

Composite	Resin (g)	TEOS (ml)	Ethanol (ml)	Water (ml)	Bent (g)
C	6	12	12	6	0
C-Bent	6	12	12	6	4.8

The cogelling used is a liquid phenol-formaldehyde commercial resin (R): liquid phenolic resin F-919 (Foundry Resins S.A) is a resole copolymer of phenol/formaldehyde in aqueous base.

The bentonite used, coming from the North Patagonia of Argentina, is constituted in 97.4% by montmorillonite, whose main properties are: CEC 105 meq/100 g, specific surface area 110 and 814 m^2/g (measured by nitrogen and water technique respectively), pH 7.1 and isoelectric point at pH 3.6. The detailed descriptions are in previous publications [43,44]. Prior to performing the tests, all the samples were previously dried at 60 °C until constant weight.

Preparation of composites

The composition of the formulations of compounds C and C-Bent was detailed in Table 1.

For the preparation of C composite, the previously described T and R were mixed on a magnetic stirrer until an emulsion was obtained, then commercial ethyl alcohol (96%) was gradually added until obtaining translucent amber liquid and finally distilled water was added.

The same procedure was followed to prepare the C-Bent composite, but previously during the synthesis development process, different ways of incorporating Bent into the R, T and ethanol mixture were tried. For example, bentonite was sonicated in water to achieve an homogeneous mixture but this limited the formation of the gel since it competes for water. Therefore, it was decided to carry out a thermal treatment at 300 °C for 72 h to dehydrate the bentonite interlayer before adding it to the pre-gel.

The different pre-gelled liquids were placed in cylindric jars of polyvinyl chloride capped at the bottom and top to prevent the gel from spilling and also to promote the syneresis process. Approximately, after 15 min the samples gelled, although they were left 24 h at room temperature without evaporation of the solvents (alcohol and water). After that time, they were uncovered allowing the evaporation of them for between 24 and 48 h. When the syneresis process was finished the samples were ready to be removed from the mold, once unmould they aged at room temperature for 24 h more. Finally, the curing process was carried out by a thermal treatment with a heating rate of 0.5 °C/min from 25 to 270 °C and maintaining the final temperature for 60 min. Lower curing temperatures were also tested, for example 180 °C, but at these temperatures it was seen that the composite leached resin at the time of the adsorption-desorption tests. Therefore, it was obtained at 270 °C as the curing temperature since it does not affect the Bent structure and the resin polymerizes and solidifies, finally obtaining the monolithic composites. A schematic diagram of the synthesis to obtain C-Bent was shown in Fig. 1.

The composites C and C-Bent were made by triplicates to evaluate the reproducibility of this technique.

Characterization

X-ray diffraction (XRD) patterns were obtained using a Philips PW-3710 diffractometer with Cu-Kα radiation (λ = 0, 154 nm) at 35 kV and 40 mA ranging from 3° to 70° 2θ.

Fourier transform infrared spectroscopy (FTIR) were performed using a Nicolet 380 spectrophotometer, obtaining transmission spectra in the area 4000–400 cm^{-1}; the samples were prepared in KBr supported pellets.

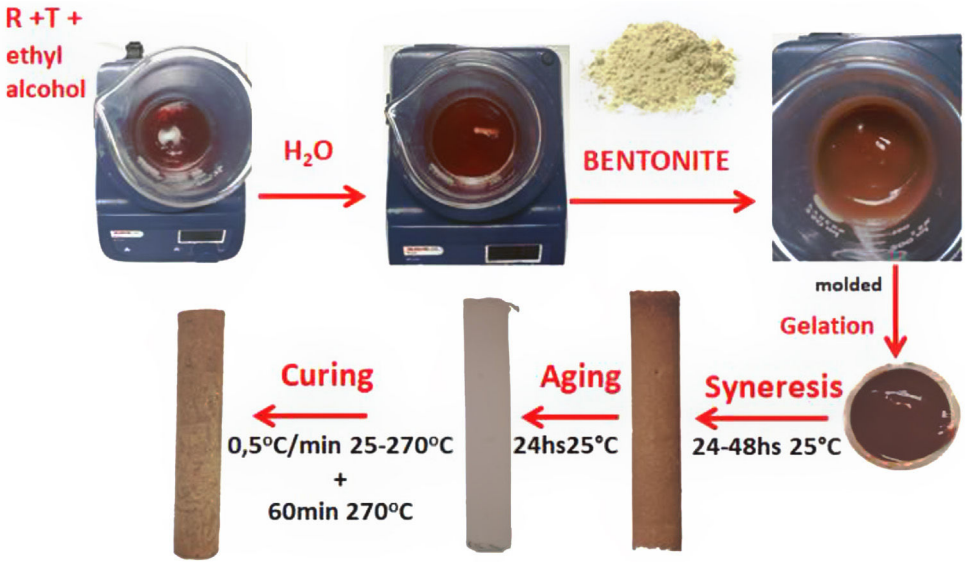

Fig. 1 – Preparation of the C-Bent.

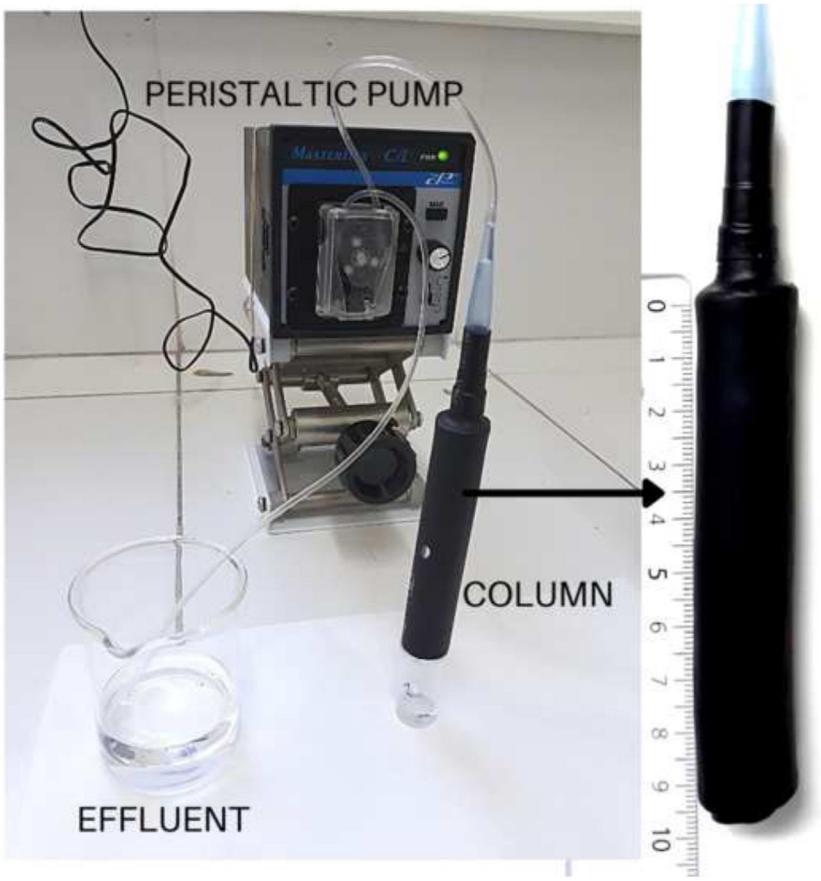

Fig. 2 – Adsorption system.

Differential thermal analysis (DTA) and thermogravimetric (TG) analysis, both thermal analyses were carried out simultaneously at 10 °C/min heating rate in air atmosphere up to 1050 °C using α-alumina as reference (Rigaku Thermo plus EVO2).

Mercury intrusion porosimetry was performed by both Porosimeter Pascal-Thermo Fisher 440 and Pascal-Thermo Fisher 140.

Adsorption of N_2 was done in a Micromeritics ASAP 2020 analyzer, and Adsorption of water vapor was measured by relative humidity technique.

Scanning electron microscopy (SEM) photographs were obtained with a JEOL CM-600 Neo Scope.

Preliminary comparative evaluation of the adsorption capacity

The monolith composites C and C-Bent were obtained as cylinders of 9 cm length by 2 cm diameter, being the mass content in C = 7.6 g, while in C-Bent = 11.2 g (bentonite mass content = 4.8 g).

Composites C and C-Bent were tested as filter beds eluting a diphenyalmine solution with a concentration of 200 ppm at a flow rate of 1 ml/min. For this the composite was introduced into a heat-shrinkable hose that connects to its external structure, forcing the effluent to pass only through the interior of the composite and also made it possible to adapt the column to the hose of the peristaltic pump (MasterFlex C/L) through which the effluent is supplied. In order to unite the different diameters of the hose and the composite, a pipette tip is added (Fig. 2). The adsorption test was carried out continuously for 8 h to simulate an industrial application, and subsequently the desorption was carried out, changing the diphenyalmine solution for distilled water and maintaining the same operation conditions for 4 h.

The eluted concentration was quantified by UV–vis spectroscopy with a Hewlett Packard 8453

Results and discussion

The sol–gel reaction of the precursors, T and R, together with the subsequent stages of condensation and polymerization during aging and curing, give rise to a network structure that is the C composite. The same occurs with the Bent addition and the preparation of C-Bent composite, but in this case the montmorillonite reactive sites participate and enhance the crosslinking process consolidating the hybrid matrix [45,46]. In this study, both composites C and C-Bent, and the individual precursor Bent were characterized.

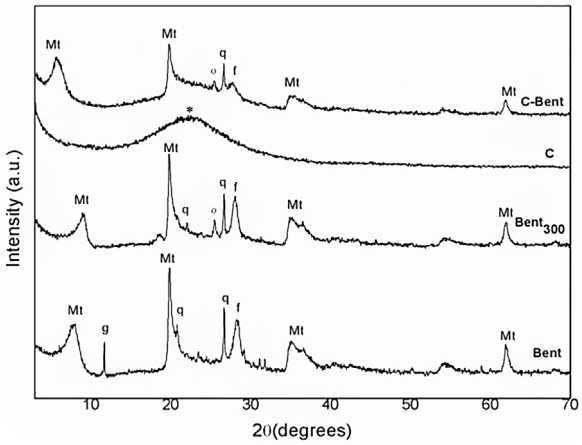

Fig. 3 – Difractograms of Bent, $Bent_{300}$, C and C-Bent, m: montmorillonite, g: $CaSO_4{\cdot}2H_2O$, q: quartz, f: feldspar, ⋆: band of amorphous silica, and o: $CaSO_4$.

Mineralogical and structural analyses

XRD

The diffraction patterns of Bent at 60 °C and thermally treated Bent 300 °C ($Bent_{300}$), were analyzed and compared by the shown reflections of montmorillonite and the accompanying minerals such as quartz (at positions 20.8° and 26.8° 2θ), gypsum (in the 11.0° 2θ, which disappears as a result of the thermal treatment in $Bent_{300}$), and feldspar (in the 28.4° 2θ) in Fig. 3. The reflection *d* (001) in position 7.9° 2θ characteristic of the dry montmorillonite at 60 °C, comparing with the one at 9.1° 2θ due to the drying at 300° C indicates the lower presence of water in the interlaminar space being 11.2 and 9.7 Å respectively.

The diagram of composite C (Fig. 3) presents a single band that is attributed to the amorphous silica centered at 23° 2θ due to the dehydrated TEOS that overlaps the amorphous reflection coming from the resin.

The diagram of composite C-Bent (Fig. 3) shows the (001) plane peak, characteristic of montmorillonite, shift to lower angles 5.6° 2θ (15.4 Å) indicating the expansion of the interlaminar space [47]. This evidence a significant expansion-exfoliation of the interlayer spacing during the stage of the sol–gel reactions that after thermal curing remains fixed and pillared montmorillonite.

There are many reactions involved in the formation of the hybrid composite, as the complete hydrolysis of TEOS, the condensation of the hydroxyl groups (—OH) in the organic and inorganic precursors with the hydroxyl groups (—OH) of montmorillonite layers edges. The large continuous network as it grows probably penetrates the interlayer and expands the spacing *d* (001) that after the aging and curing stages remains swollen.

The pillared montmorillonite provides the available space for adsorption processes and at the same time keeps the interlayer fixed avoiding swelling of the montmorillonite in the composite matrix. This last, is one of the objectives sought for its application as monolithic composite in fixed beds columns.

It was also observed that the peaks corresponding to bentonite, montmorillonite and other minerals, although they overlap the amorphous silicon band, preserved their structure.

In $Bent_{300}$ and C-Bent diffractograms, both samples treated at 300 °C, appears a peak at the position of 25.6° 2θ corresponding to anhydrite mineral ($CaSO_4$) formed by the dehydration of gypsum ($CaSO_4{\cdot}2H_2O$) occurred at temperatures lower than 200 °C.

DTA-TG

The DTA of Bent and the composites (Fig. 4a), were analyzed, Bent presented two endothermic bands that allows explaining the correspondence to the loss of water from montmorillonite interlayer at 76 °C and hydration water of Gypsum at 127 °C. The endothermic band at 660 °C corresponds to the dehydroxylation (loss of OH—) of the montmorillonite structure [48].

In the corresponding C composite curve is also observed a first endothermic band (53 °C) corresponding to the water captured during the conditioning of the samples, and a second exothermic band consisting of two peaks at 433 and 475 °C product of the decomposition and oxidation of the organic compounds coming from R and the main part of the combustion of it. Also, an exothermic peak at 998 °C with a mass loss of 0.7%, which corresponds to the transformation of silica (from T) to cristobalite (SiO2). This was confirmed by XRD analysis, carrying C to a thermal treatment at 1050 °C for one hour.

The C-Bent composite curve is similar to the C composite curve, with an endothermic band at 61 °C attributable to the humidity captured by the sample in the conditioning and a large exothermic band at 450 °C. This band is composed of two exothermic processes with mass loss of 12.5% and 3.3%, shown in the TG analysis being the interpretation analogous to the composite C, but with a widened band that involve the two processes mentioned above.

From Fig. 4b of thermogravimetric analysis, it is observed that composite C presents a mass loss of 22% in the band between 300 and 580 °C from the combustion of the organic matter coming from the resin according with the description of DTA. In C-Bent, the loss of mass, between 300 and 670 °C, is 15.8% and the same two peaks coming from the combustion processes of the resin (observed in C), in this case were clearly distinguished, because are separated and due to the clay interaction the peaks are delayed. The percentage of mass loss in C and C-Bent is coincident considering the proportion of resin in each one of them.

In order to a better interpretation of the results, were performed the DTA-TG analysis of each precursor R and T, under the same curing conditions (Fig. 5). When comparing the DTA of C with that of its precursors, R and T, it is observed that the decomposition of the pure resin occurs at higher temperatures than the decomposition of the organic matter in C. It could be attributed to the texture of composite C (consisting of resin, TEOS, ethanol and water) that has a porous structure obtained from the release of the solvents in the curing stage unlike the cured resin resulting in a closed and compact structure. Therefore, O_2 diffuses more rapidly through the pores of C, so combustion occurs at lower temperatures than in the case of resin with a compact structure. In the case of C-Bent, the temperature delay in the degradation of the resin could be justified by a decrease in the porosity given by the addition of

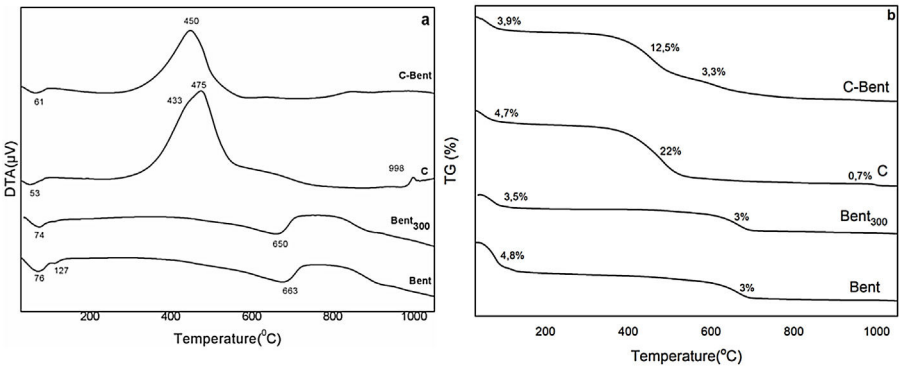

Fig. 4 – (a) Differential thermal analysis curves; (b) thermogravimetric analysis curves of Bent, $Bent_{300}$, C, C-Bent.

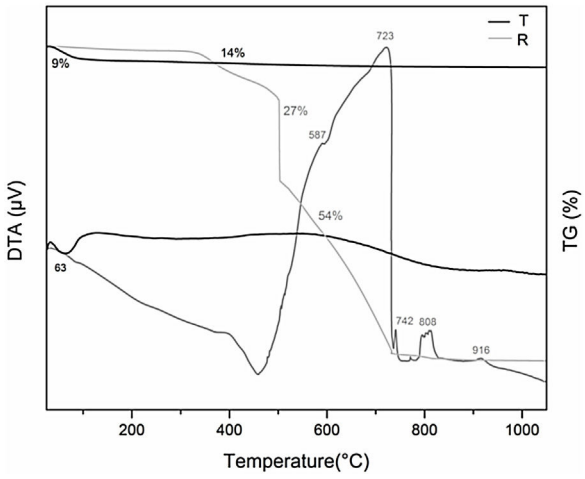

Fig. 5 – Differential thermal analysis and thermogravimetric analysis curves of R and T precursors.

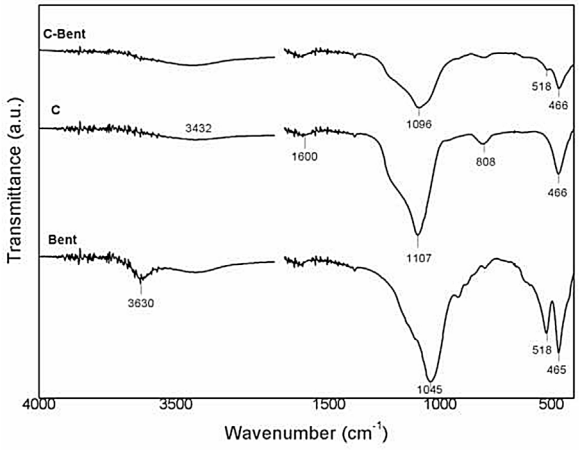

Fig. 6 – FTIR spectra of the composites Bent, C, and C-Bent.

Bent, which was verified by porosimetry. From the TG curves was observed that the mass loss until 300 °C by the precursors T and R, is due to the dehydration, so that C and C-Bent, during the thermal curing only dry without modifying their structure.

FTIR

IR Spectra of Bent and the composites obtained are shown in Fig. 6. In the case of Bent spectrum is typical of bentonite, with two strong signals at 465 and 518 cm^{-1} belong to the vibration of Si—O in the tetrahedral layer and the Si—O—Al in the octahedral layer respectively in the montmorillonite. While weak signals are observed at 790 cm^{-1} related to Si—O vibration characteristic of quartz, and at 920 cm^{-1} attributed to Al—OH groups in the octahedral layer in the montmorillonite. The signal at 1045 cm^{-1} corresponds to Si—O of the tetrahedral layer in montmorillonite. The band at 3432 cm^{-1} is due to the H—OH vibrations of the water adsorbed on the interlayer structure and the band at 3630 cm^{-1} is attributed to Al—OH stretching of the octahedral layer, both in montmorillonite [49].

The spectra of the composites are similar between each other, although the effect of a slight dilution due to the added bentonite. In composite C the signals in 466 and at 808 cm^{-1} were related to the Si—O—Si unions from condensation of TEOS, the signal at 1107 cm^{-1} is assigned to Si—O—R from TEOS but there is other signal inside (1230 cm^{-1}) corresponding to C—C=O group from the phenolic resin. The broad signal at 3450 cm^{-1} is related to the stretching vibrations of OH in the aromatic ring (C—OH) coming all from the resin due to the hydration process during the sample conditioning process. The differences found in C-Bent from C spectrum is the signal at 518 cm^{-1} corresponding to the vibration of Si—O in the tetrahedral layer of the montmorillonite and also an even wider band at 1096 cm^{-1} that is composed by the signal (1107 cm^{-1}) of Si—O—R group from TEOS, the signal (1230 cm^{-1}) corresponding to C—C=O group from the phenolic resin and the signal (1045 cm^{-1}) of Si—O of the tetrahedral layer in montmorillonite [50–52].

Texture analyses

Mercury porosimetry

The pore size distribution curves evaluated by mercury accumulative intrusion vs. pore size and their derivatives were presented in Fig. 7. A continuous distribution between 10 and 10,000 nm and a total pore volume below the others (200 mm^3/g) was showed by Bent. While C showed a wide pore size distribution in the range of meso-macropores between 50 and 14,000 nm with three modes, at 120, 2000 nm and a

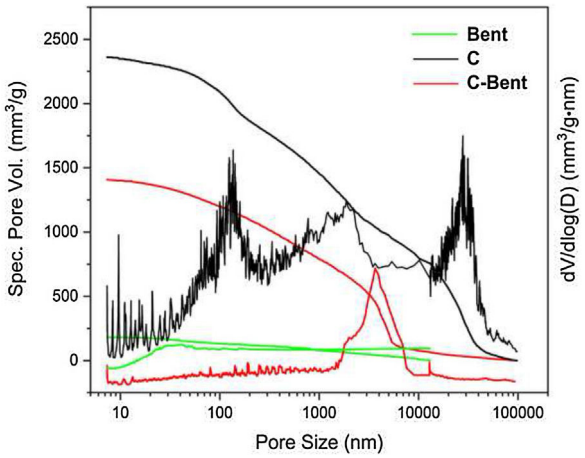

Fig. 7 – Accumulated pore volume (mm^3/g) vs pore size (nm) of Bent, C and C-Bent and their derivatives.

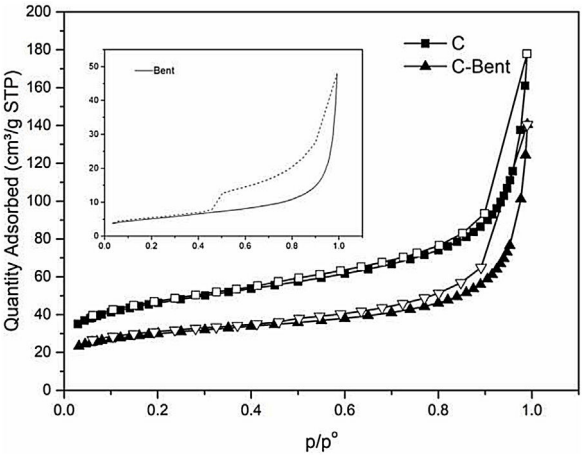

Fig. 8 – Adsorption–desorption isotherms of Bent, C and C-Bent.

significant one at 30,000 nm. When these were compared to C-Bent, the pore volume decreased due to the addition of Bent. Probably, it occurs because the pores of C were filled with the bentonite homogenizing the wide pore size distribution for C-Bent in a single mode at 3500 nm.

Nitrogen adsorption

The analyses of the experimental nitrogen isotherms of adsorption-desorption are carried out for Bent, C and C-Bent to investigate the texture of the composites surface. In Fig. 8 adsorption–desorption curves are shown to compare and analyze the differences and due to the behaviors found can be classified as type IV [53–55]. As it is known and shown Bent presents the typical hysteresis cycle of laminar pores as it is with montmorillonites. The shape of the isotherms C and C-Bent indicate a narrow and large type of pore, where C adsorbed a greater amount of N_2 than C-Bent and the interaction of bentonite in C-Bent modifies the behavior of the isotherm showing a cycle of hysteresis with certain laminarity in the pore.

The textural characteristics (Table 2) where composite C presents the highest value of BET specific surface being 164 m^2/g, while the addition of bentonite generates a decrease in the evaluation of the specific surface area. Also, in C-Bent, the pore volume decrease from C due to the addition of bentonite and in accordance with what is observed in Fig. 8, bentonite filled C porous decreasing the total pore volume and also the specific surface area. The BET analyses do not allow giving a pore mean diameter because they present a continuous distribution in the mesoporous region. But the c constant related with the energetic interaction between adsorbate–absorbent, present the highest value for C-Bent and could be attributed at the montmorillonite charge density concentration inside the original C pores.

Water adsorption

The evaluation of the specific surface by water vapor was carried out, as an indicative measure of the interaction capacity of the composite with water for further applications. It was carried out in a controlled atmosphere at 53% humidity (saturated $Na_2Cr_2O_7$ solution) at 25 °C temperature for 72 h. The relative humidity chosen corresponds to the formation of a monolayer of water on the surface of the solid [56–58] and the results are presented in Table 2.

Bent has the highest value of specific surface by water adsorption being 1187 m^2/g, and it is attributed at the polarity of the water molecule to probe the charged surface of the montmorillonite. Following the same order as with N_2, C-Bent has the lowest surface value than C attributable to bentonite covering-blocking certain pores of C.

SEM

According to the microscope used and to be able to compare between sample structures, the micrographs were taken with 1000× magnification. It should be noted that with this magnification was not possible to observe the typical laminar structure of montmorillonite due to its nanometric size.

Fig. 9.1 shows the coral-like structure related with the solvent release, resulting a structure with spongy appearance constituted by the composite (T/R) where spherical/cylindrical channels or gaps of dimensions between 1000 and 5000 nm are observed. On the other hand, in Fig. 9.2 a more compact structure can be seen without being the characteristic laminar structure of the clay, but neither that which is observed in Fig. 9.1 regarding the composition of C. In this case the empty spaces that are observed in the spongy structure is approx. 2000 nm in a hybrid morphology between sheets (such as those presented by clays) and a spongy structure (such as that presented by C).

Comparative preliminary evaluation of the adsorptive capacity of C-Bent

From the textural results, which shown a lower specific surface of C-Bent compared with C, preliminary comparative adsorption tests were carried out to evaluate the composites according to the future applications of C-Bent as filter bed.

The performance of a fixed bed column is obtained through the breakthrough curve (BTC) [59]. In order to predict the BTC of both composites and determined the column kinetic

Table 2 – Textural parameters evaluated by N_2, S.BET (specific surface), Vt (total volume of pores) and c (energetic constant); and S.H_2O (specific surface measured by H_2O).

Composite	S.BET (m^2/g)	Vt (cm^3/g)	c	S.H_2O(m^2/g)
C	167	0.22	265	778
C-Bent	95	0.13	330	464
Bent	18	0.05	160	1187

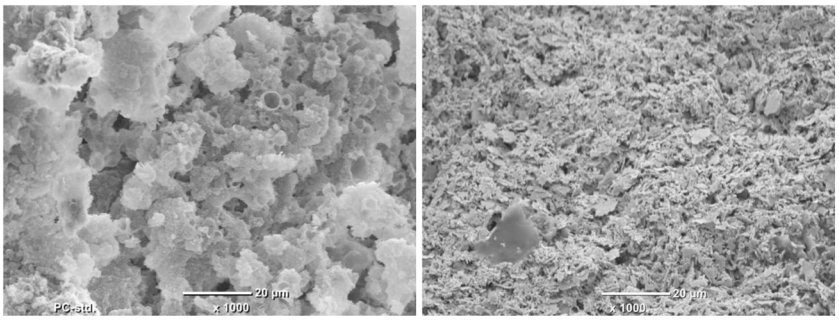

Fig. 9 – (1) SEM image of C ×1000. (2) SEM images of C-Bent ×1000.

Table 3 – Comparative breakthrough curve parameters (Thomas model) of C and C-Bent fixed bed column for dyphenilamine adsorption.

Column	C_0 (mg/L)	Q (ml/min)	Z (cm)	X (g)	t_b (min)	t_e (min)	k_{Th} (ml/min mg)	q_0 (mg/g)	R^2
C	200	1	9.5	7.6	25	100	0.55	1.1	0.99
C-Bent	200	1	9.5	11.2	55	100	0.98	1.4	0.93

Table 4 – Comparative diphenylamine adsorption–desorption results of fixed bed column C and C-Bent.

Column	Maximum operation time (h)	Maximum adsorption (%)	Desorption (%)
C	4	65–78	70
C-Bent	6	73–90	15

parameters, the Thomas model (Eq. (1)) were applied to the experimental data obtained from dynamic studies [60]. Following this, initial concentration (200 ppm) of a diphenylamine solution was eluted in C and C-Bent columns of monilithic composite at a flow rate of 1 ml/min:

$$\frac{C_e}{C_0} = \frac{1}{1 + \exp(k_{Th}/Q)(q_0 X - C_0 V_{eff})} \quad (1)$$

In Eq. (1), k_{Th} is the rate constant (ml/min mg), q_0 is the maximum solid-phase concentration of the solute (mg/g), X is the amount of adsorbent in the column (g), C_0 is the inlet concentration (mg/L), C_e is the effluent concentration (mg/L), Q is the flow rate (ml/min) and V_{eff} is the effluent volume (ml).

From the BTC of C and C-Bent (provided as supplementary information), the parameters (Thomas model) were obtained and presented in Table 3. The breakthrough time (t_b) is obtained at $C_e/C_0 = 0.1$ showing a significant shift of C-Bent (55 min) to greater values comparing with C (25 min) while the time of exhaustion (t_e) it is almost the same (100 min) for both composites. The higher value of k_{Th} for C-Bent indicates high adsorption rate caused by bentonite that would give a catalytic effect. Also the higher value of q_0 for C-Bent shows the incremental adsorption given by the mass of bentonite.

So, although the specific surface value was lower for C-Bent, the adsorption capacity was higher.

The percentage of adsorption-desorption was also compared between composites and the results are displayed in Table 4. The adsorption capacity of C-Bent achieves the maximum of 73–90% while C only reaches 65–78%. This difference in the range of the adsorption capacity is given by the dispersion inherent to the experimental work, as flow variations due to mechanical and textural aspects of the column because of the distribution of the Bent within the composite. The big difference was found in desorption capacity where the maximum was 15% for C-Bent and 70% for C reached in 1 hour of operation. This reveals that the adsorption in C-Bent would present a stronger bond between the adsorbate and the adsorbent binding sites, which could be explained as a physical adsorption occurs in C, given by the spongy and porous structure of the material, without generating adsorbent interaction, so it is easily removed in contact with the flow of water. On the other hand, C-Bent, as a hybrid material, could have a synergistic adsorption effect in which physical and chemical adsorption occurs. The physical adsorption given by the primary composite and the chemical given by bentonite, predominating the latter in the desorption process.

As preliminary results they are promising to continue in future work.

It should be noted that structurally the monolith C-Bent remains operative (continuous constant flow rate for more than 6 h) while monolith C barely reaches 4 h of operation and drastically decreased the flow rate.

Conclusions

A porous monolithic hybrid composite, C-Bent, with the maximum rate of Bent (21%, w/w) was prepared by sol–gel technique, and despite the low repetitiveness of other products obtained in general by this technique, this one was reproduced several times without significant differences. From the characterization carried out of C and C-Bent composites, it was shown that Bent interacts within the precursors of the composites during the sol–gel and curing process fixing the montmorillonite interlaminar spacing. It was observed that Bent tends to be located in the macro/mesopores of the structure granted by the T/R network, which enhances its adsorption properties, due to a concentration of charge density in the pores that increases its adsorption capacity. Although C has a higher specific surface than C-Bent, it is the montmorillonite in C-Bent responsible for maximizing the adsorption capacity of the adsorbate used for the test which is an emerging pollutant.

It was achieved that montmorillonite in C-Bent monolith maintains its adsorption capacity with a controlled and fixed swelling. These results are promising to continue studying the performance of C-Bent in treating aqueous effluents contaminated with emerging pollutants.

Acknowledgements

The Argentinian agencies Consejo Nacional de Investigaciones Científicas y Técnicas (CONICET) and Comisión de Investigaciones Científicas (CIC) are acknowledged for financial support.

Appendix A. Supplementary data

Supplementary data associated with this article can be found, in the online version, at doi:10.1016/j.bsecv.2021.10.001.

REFERENCES

[1] M. Nazir, M. Kassim, L. Mohapatra, M. Gilani, M. Raza, K.K. Majeed, Characteristic properties of nanoclays and characterization of nanoparticulates and nanocomposites, in: M. Jawaid, A. Qaiss, R. Bouhfid (Eds.), Nanoclay Reinforced Polymer Composites. Engineering Materials, Springer, Singapore, 2016, pp. 35–55, http://dx.doi.org/10.1007/978-981-10-1953-1_2.

[2] H. Patel, R. Somani, H. Bajaj, R. Jasra, Nanoclays for polymer nanocomposites, paints, inks, greases and cosmetics formulations, drug delivery vehicle and waste water treatment, Bull. Mater. Sci. 29 (2006) 133–145.

[3] D. Paul, L. Robeson, Polymer nanotechnology: nanocomposites, Polymer 49 (2008) 3187–3204, http://dx.doi.org/10.1016/j.polymer.2008.04.017.

[4] N. Kantesaria, S. Sharma, Exfoliation and extraction of nanoclay from montmorillonite mineral rich bentonite soil, in: A. Prashant, A. Sachan, C. Deasi (Eds.), Advances in Computer Methods C. Geomechanics Lecture Notes in Civil Engineering, vol. 56, Springer, Singapore, 2020, pp. 1–12, http://dx.doi.org/10.1007/978-981-15-0890-5_1.

[5] M. Khoeini, S. Bazgir, M. Tamizifar, A. Nemati, K. Arzani, Investigation of the modification process and morphology of organosilane modified nanoclay, Ceramics-Silikáty 53 (2009) 254–259.

[6] F. Bergaya, G. Lagaly, General introduction: clays, clay minerals, and clay science, in: F. Bergaya, B. Theng, G. Lagaly (Eds.), Handbook of Clay Science: Developments in Clay Science, vol. 1, Elsevier, Amsterdam, 2006, pp. 1–18, http://dx.doi.org/10.1016/S1572-4352(05)01001-9.

[7] F. Bergaya, Layered clay minerals. Basic research and innovative composite applications, Microporous Mesoporous Mater. 107 (2008) 141–148.

[8] S. Shaikh, M. Nasser, I. Hussein, A. Benamor, S. Onaizi, H. Qiblawey, Influence of polyelectrolytes and other polymer complexes on the flocculation and rheological behaviors of clay minerals: acomprehensive review, Sep. Purif. Technol. 187 (2017) 137–161.

[9] A. Kausar, M. Iqbal, A. Javed, K. Aftab, H. Bhatti, S. Nouren, Dyes adsorption using clay and modified clay: a review, J. Mol. Liq. 256 (2018) 395–407.

[10] F. Uddin, Clays nanoclays, and montmorillonite minerals, Metall. Mater. Trans. A 39 (2008) 2804–2814, http://dx.doi.org/10.1007/s11661-008-9603-5.

[11] H. Murray, Bentonite applications, in: H. Murray (Ed.), Developments in Clay Science, vol. 2, Elsevier, 2006, pp. 111–130, http://dx.doi.org/10.1016/S1572-4352(06)02006-X (Chapter 6).

[12] P. Loganathan, S. Vigneswaran, J. Kandasamy, Enhanced removal of nitrate from water using surface modification of adsorbents – a review, J. Environ. Manag. 131 (2013) 363–374.

[13] D. Manning, Handbook of clay science, in: F. Bergaya, B.K.G. Theng, G. Lagaly (Eds.), European Journal of Soil Science, vol. 58, 2007, pp. 518–519, http://dx.doi.org/10.1111/j.1365-2389.2007.00898_4.

[14] G. Lagaly, Pesticide-clay interactions and formulations, Appl. Clay Sci. 18 (2001) 205–209, http://dx.doi.org/10.1016/S0169-1317(01)00043-6.

[15] S. Azarkan, K. Aranzazu, D. Khalid, I. Sainz-Diaz, Adsorption of two fungicides on natural clays of Morocco, Appl. Clay Sci. 123 (2016) 37–46.

[16] L. Zhu, R. Zhu, Simultaneous sorption of organic compounds and phosphate to inorganic–organic bentonites from water, Sep. Purif. Technol. 54 (2007) 71–76.

[17] R. Zhu, Q. Chen, Q. Zhou, Y. Xi, J. Zhu, H. He, Adsorbents based on montmorillonite for contaminant removal from water: a review, Appl. Clay Sci. 123 (2016) 239–258, http://dx.doi.org/10.1016/j.clay.2015.12.024.

[18] J. Cornejo, R. Celis, I. Pavlovic, M. Ulibarri, Interactions of pesticides with clays and layered double hydroxides: a review, Clay Miner. 43 (2008) 155–175, http://dx.doi.org/10.1180/claymin.2008.043.2.01.

[19] J. Brixie, S. Boyd, Treatment of contaminated soils with organoclays to reduce leachable pentachlorophenol, J. Environ. Qual. 23 (1994) 1283–1290.

[20] M. Sánchez-Martín, M. Rodríguez-Cruz, M. Andrades, M. Sánchez-Camazano, Efficiency of different clay minerals

modified with a cationic surfactant in the adsorption of pesticides: influence of clay type and pesticide hydrophobicity, Appl. Clay Sci. 31 (2006) 216–228.
[21] W. Zheng, S. Papiernik, M. Guo, R. Dungan, S. Yates, Construction of a reactive surface barrier to reduce fumigant 1,3-dichloropropene emissions, Environ. Toxicol. Chem. 24 (2005) 1867–1874.
[22] E. Koutsopoulou, D. Papoulis, P. Tsolis-Katagas, M. Kornaros, Clay minerals used in sanitary landfills for the retention of organic and inorganic pollutants, Appl. Clay Sci. 49 (2010) 372–382.
[23] A. Carrado, Synthetic body – and polymer-clays: preparation, characterization, materials and applications, Appl. Clay Sci. 17 (2000) 1–23, http://dx.doi.org/10.1016/S0169-1317(00)00005-3.
[24] K. Hernández-Hernández, J. Illescas, M. Díaz-Nava, S. Martínez-Gallegos, C. Muro-Urista, R. Ortega-Aguilar, E. Rodríguez-Alba, E. Rivera, Preparation of nanocomposites for the removal of phenolic compounds from aqueous solutions, Appl. Clay Sci. 14 (2018) 212–217.
[25] Z. Qian, G. Hu, S. Zhang, M. Yang, Preparation and characterization of montmorillonite-silica nanocomposites: a sol–gel approach to modifying clay surfaces, Physica B: Condens. Matter 18 (2008) 3231–3238, http://dx.doi.org/10.1016/j.physb.2008.04.008.
[26] A. Sadanand Pandey, Comprehensive review on recent developments in bentonite-based materials used as adsorbents for wastewater treatment, J. Mol. Liq. 241 (2017) 1091–1113.
[27] A. Awad, S. Shaikh, R. Jalab, M. Gulied, M. Nasser, A. Benamor, S. Adham, Adsorption of organic pollutants by natural and modified clays: a comprehensive review, Sep. Purif. Technol. 228 (2019) 115719, http://dx.doi.org/10.1016/j.seppur.2019.115719.
[28] C. Lazaratou, D. Vayenas, D. Papoulis, The role of clays, clay minerals and clay-based materials for nitrate removal from water systems: a review, Appl. Clay Sci. 185 (2020) 105377.
[29] D. Ghernaout, B. Ghernaout, Sweep flocculation as a second form of charge neutralization, J. Desal. Water Treat. 44 (2012) 1–3.
[30] M. Hossein, The separation method for removing of colloidal particles from raw water, Am.-Euras. J. Agric. Environ. Sci. 4 (2008) 266–273.
[31] P. Luckham, S. Rossi, The colloidal and rheological properties of bentonite suspensions, Adv. Colloid Interface Sci. 82 (1999) 43–92, http://dx.doi.org/10.1016/S0001-8686(99)00005-6.
[32] S. Starodoubtsev, A. Ryabova, A. Dembo, K. Dembo, I. Aliev, A. Wasserman, A. Khokhlov, Composite gels of poly (acrylamide) with incorporated bentonite. Interaction with cationic surfactants, ESR and SAXS study, Macromolecules 35 (2002) 6362–6369, http://dx.doi.org/10.1021/MA012021Z.
[33] W. Moa, Q. Hea, X. Sua, S. Maa, J. Fenga, Z. Heb, Preparation and characterization of a granular bentonite composite adsorbent and its application for Pb2+ adsorption, Appl. Clay Sci. 159 (2018) 68–73.
[34] K. He, G. Zeng, A. Chen, Z. Huang, M. Peng, T. Huang, G. Chen, Graphene hybridized polydopamine-kaolin composite as effective adsorbent for methylene blue removal, Compos. Part B: Eng. 16 (2019) 141–149.
[35] M. Awual, Novel ligand functionalized composite material for efficient copper (II) capturing from wastewater sample, Compos. Part B: Eng. 172 (2019) 387–396.
[36] A. Ghribi, M. Bagane, Removal of Rhodamine B from aqueous solution using natural clay by fixed bed column method, Int. J. Chem. Mol. Eng. 10 (2016) 94–97.
[37] E. Dragan, M. Dinu, Biopolymers-zeolites composites as biosorbents for separation processes, in: E. Dragan (Ed.), Advanced Separations by Specialized Sorbents, CRC Press, 2014, pp. 145–175, http://dx.doi.org/10.1201/b17426-7.
[38] A. Scian, C. Volzone, Novel SiO_2C composite material, Bol. Soc. Esp. Cerám. Vidrio 40 (2001) 279–284.
[39] M. Seeni Meera, R. Murali Sankar, A. Murali, A. Jaisankar, A. Mandal, Sol–gel network silica/modified montmorillonite clay hybrid nanocomposites for hydrophobic surface coatings, Colloids Surf. B: Biointerfaces 90 (2012) 204–210, http://dx.doi.org/10.1016/j.colsurfb.2011.10.018.
[40] X. Yu, S. Ding, Z. Meng, J. Liu, X. Qu, Y. Lu, Z. Yang, Aerosol assisted synthesis of silica/phenolic resin composite mesoporous hollow spheres, Colloid Polym. Sci. 286 (2008) 1361–1368.
[41] F. Calvo-Flores, J. Isaac-García, J. Dobado, Emerging Pollutants: Origin, Structure, and Properties, John Wiley & Sons (2018), http://dx.doi.org/10.1002/9783527691203.
[42] A. Scian, G. Suarez, E. Moyas, B. Lombardi, Treatment of agroindustrial liquid effluents, in: II International Congress of Environmental Science and Technology and II National Congress of the Argentine Society of Environmental Science and Technology (SACyTA) Buenos Aires, 2015.
[43] B. Lombardi, M. Baschini, R. Torres Sánchez, Characterization of montmorillonite from North Patagonia (Argentina) deposits: physicochemical and structural parameters correlation", J. Argentine Chem. Soc. (2002) 87–99.
[44] B. Lombardi, M. Baschini, R.R. Torres Sánchez, Bentonite deposits of Northern Patagonia, Appl. Clay Sci. 845 (2003) p.1–p.4.
[45] A. Bourlinos, D. Jiang, E. Giannelis, Clay–organosiloxane hybrids: a route to cross-linked clay particles and clay monoliths, Chem. Mater. 16 (2004) 2404–2410.
[46] J. Dai, J. Huang, Surface modification of clays and clay–rubber composite, Appl. Clay Sci. 15 (1999) 51–65.
[47] G. Brown, W. Brindley, Crystal structures of clay minerals and their X-ray identification, Mineral. Soc. Great Britain Ireland London UK 5 (1980), http://dx.doi.org/10.1180/mono-5.
[48] Q. Zuo, X. Gao, J. Yang, P. Zhang, G. Chen, Y. Li, W. Wu, Investigation on the thermal activation of montmorillonite and its application for the removal of U (VI) in aqueous solution, J. Taiwan Inst. Chem. Engrs. 80 (2017) 754–760.
[49] S. Gammoudi, N. Frini-Srasra, E. Srasra, Influence of exchangeable cation of smectite on HDTMA adsorption: equilibrium, kinetic and thermodynamic studies, Appl. Clay Sci. 69 (2012) 99–107.
[50] G.G. Socrates, Infrared and Raman Characteristic Group Frequencies, 3rd ed., John Willey & Sons Ltd Press, West Sussex, UK, 2001.
[51] I. Poljansek, M. Krajnc, Characterization of phenol-formaldehyde prepolymer resins by in line FT-IR spectroscopy, Acta Chim. Slov. 52 (2005) 238–244.
[52] V. Farmer, Infrared spectra of minerals, Mineral. Soc. Great Britain Ireland London UK 4 (1974), http://dx.doi.org/10.1180/mono-4.
[53] K. Sing, D. Everett, R. Haul, L. Moscou, R. Pierotti, J. Rouquerol, T. Siemieniewska, Reporting physisorption data for gas/solid system, Pure Appl. Chem. 57 (1985) 603–619, http://dx.doi.org/10.1351/pac198557040603.
[54] V. Zivica, M. Palou, Physico-chemical characterization of thermally treated bentonite, Compos. Part B: Eng. 68 (2015) 436–445.
[55] T. Khalil, S. Chaabene, S. Boujday, J. Blanchard, L. Bergaoui, A new method for elaborating mesoporous SiO_2/montmorillonite composite materials, J. Sol–Gel Sci. Technol. 75 (2015) 436–446.

[56] C. Hatch, J. Wiese, C. Crane, K. Harris, H. Koss, J. Baltrusaitis, Water adsorption on clay minerals as a function of relative humidity: application of BET and Freundlich adsorption models, Langmuir 28 (2012) 1790–1803.
[57] J. Cases, I. Berend, G. Besson, M. Francois, M. Uriot, F. Thomas, J. Poirier, Mechanism of adsorption and desorption of water vapor by homoionic montmorillonite. The sodium-exchanged form, Langmuir 8 (1992) 2730–2739.
[58] J. Rouquerol, F. Rouquerol, P. Llewellyn, G. Maurin, K. Sing, Adsorption by Powders and Porous Solids: Principles, Methodology and Applications, 2nd ed., Academic Press, Elsevier, 2012, http://dx.doi.org/10.1016/C2010-0-66232-8.
[59] R. Han, Y. Wang, X. Zhao, Y. Wang, F. Xie, J. Cheng, M. Tang, Adsorption of methylene blue by phoenix tree leaf powder in a fixed-bed column: experiments and prediction of breakthrough curves, Desalination 245 (2008) 284–297.
[60] P. Kojić, V. Vučurović, N. Lukić, M. Karadžić, S. Popović, Continuous adsorption of methylene blue dye on the maize stem ground tissue, Acta Period. Technol. 48 (2017) 127–139.